THE JOURNAL OF BIOLOGICAL CHEMISTRY VOL. 288, NO. 9, pp. 6284–6294, March 1, 2013

Domain 1 of Mucosal Addressin Cell Adhesion Molecule Has an I1-set Fold and a Flexible Integrin-binding Loop*[S]

Received for publication, August 23, 2012, and in revised form, December 7, 2012 Published, JBC Papers in Press, January 7, 2013, DOI 10.1074/jbc.M112.413153

Yamei Yu[‡], Jianghai Zhu[‡], Po-Ssu Huang[§], Jia-huai Wang[¶], Nick Pullen[‖], and Timothy A. Springer[‡1]

From the [‡]Program in Cellular and Molecular Medicine, Children's Hospital Boston, and Department of Biological Chemistry and Molecular Pharmacology, Harvard Medical School, Boston, Massachusetts 02215, the [§]Department of Biochemistry, University of Washington, Seattle, Washington 98195, the [¶]Dana-Farber Cancer Institute and Department of Pediatrics, Harvard Medical School, Boston, Massachusetts 02215, and [‖]Pfizer Global Research and Development, Cambridge, Massachusetts 02140

Background: MAdCAM/$\alpha_4\beta_7$ interaction directs lymphocyte homing to mucosal tissues.
Results: Four crystal structures demonstrate large differences in the integrin-binding loop and whether a C′ or D strand is present in D1.
Conclusion: The integrin-binding loop of MAdCAM is inherently flexible.
Significance: This may reflect a specialization of MAdCAM to mediate rolling and firm adhesion by binding to different $\alpha_4\beta_7$ integrin conformations.

Mucosal addressin cell adhesion molecule (MAdCAM) binds integrin $\alpha_4\beta_7$. Their interaction directs lymphocyte homing to mucosa-associated lymphoid tissues. The interaction between the two immunoglobulin superfamily (IgSF) domains of MAdCAM and integrin $\alpha_4\beta_7$ is unusual in its ability to mediate either rolling adhesion or firm adhesion of lymphocytes on vascular surfaces. We determined four crystal structures of the IgSF domains of MAdCAM to test for unusual structural features that might correlate with this functional diversity. Higher resolution 1.7- and 1.4-Å structures of the IgSF domains of MAdCAM in a previously described crystal lattice revealed two alternative conformations of the integrin-binding loop, which were deformed by large lattice contacts. New crystal forms in the presence of two different Fabs to MAdCAM demonstrate a shift in IgSF domain topology from the I2- to I1-set, with a switch of integrin-binding loop from CC′ to CD. The I1-set fold and CD loop appear biologically relevant. The different conformations seen in crystal structures suggest that the integrin-binding loop of MAdCAM is inherently flexible. This contrasts with rigidity of the corresponding loops in vascular cell adhesion molecule, intercellular adhesion molecule (ICAM)-1, ICAM-2, ICAM-3, and ICAM-5 and may reflect a specialization of MAdCAM to mediate both rolling and firm adhesion by binding to different $\alpha_4\beta_7$ integrin conformations.

Mucosal addressin cell adhesion molecule-1 (MAdCAM)[2] is a ligand for integrin $\alpha_4\beta_7$. MAdCAM is selectively expressed on the intestinal endothelium in mucosal sites, including Peyer's patch, high endothelial venules, and postcapillary venules in lamina propria (1, 2). Binding to MAdCAM helps direct homing of $\alpha_4\beta_7^+$ lymphocytes to Peyer's patches and the intestinal lamina propria (3). In an unusual example of different classes of adhesion receptors mediating comparable functions, the integrin family molecule $\alpha_4\beta_7$ is the receptor for homing to mucosal sites, although the selectin family molecule L-selectin mediates homing to peripheral lymph nodes (4).

MAdCAM belongs to a subset of IgSF molecules that act as cell surface ligands for integrins. These include VCAM, ICAM-1, ICAM-2, ICAM-3, and ICAM-5, and crystal structures are available for all (5–12). All have two to nine IgSF domains, with N-terminal domains 1 and 2 (compared below) sufficient for integrin binding. MAdCAM and VCAM, which bind integrins $\alpha_4\beta_7$ and $\alpha_4\beta_1$, are considered one subfamily; however, they are only 23% identical in amino acid sequence, which is comparable with their level of identity with ICAMs (22%). By contrast, ICAMs, which bind to integrin $\alpha_L\beta_2$, are more closely related to one another (29–44%). MAdCAM and VCAM share an Asp-bearing loop in domain 1 and a nearby loop in domain 2 that make important contributions to α_4 integrin binding as shown with chimeras and site-directed mutagenesis (13–15).

Among these cell surface integrin ligands, MAdCAM is uniquely important in rolling adhesiveness. Whereas $\alpha_4\beta_1$ and $\alpha_L\beta_2$ integrins and their ligands VCAM and ICAMs primarily mediate firm adhesion, the primary function of $\alpha_4\beta_7$ and MAdCAM is in homing and rolling adhesion, although they also mediate firm adhesion. In rolling adhesion, the zone of adhesion between a leukocyte and the endothelium is translated downstream in response to hydrodynamic drag forces exerted on the leukocyte. Rolling adhesion can be reconstituted with MAdCAM adsorbed to artificial vessel walls. Upon activa-

* This work was supported, in whole or in part, by National Institutes of Health Grant HL103526.
[S] This article contains supplemental Figs. S1 and S2.
The atomic coordinates and structure factors (codes 4HD9, 4HBQ, 4HC1, and 4HCR) have been deposited in the Protein Data Bank (http://wwpdb.org/).
[1] To whom correspondence should be addressed: Program in Cellular and Molecular Medicine, Children's Hospital Boston, and Department of Biological Chemistry and Molecular Pharmacology, Harvard Medical School, 3 Blackfan Circle, Boston, MA 02115. Tel.: 617-713-8200; Fax: 617-713-8232; E-mail: springer@idi.harvard.edu.
[2] The abbreviations used are: MAdCAM, mucosal addressin cell adhesion molecule; IgSF, immunoglobulin superfamily; ICAM, intercellular adhesion molecule; TEV, tobacco etch virus; MIDAS, metal ion-dependent adhesion site; VCAM, vascular cell adhesion molecule; r.m.s.d., root mean square deviation.

tion, leukocytes become firmly adhesive through integrins, *i.e.* rolling is halted and the integrins mediate cell spreading and migration (4). Intermediate and open conformations of the $\alpha_4\beta_7$ headpiece may mediate rolling and firm adhesion, respectively (16). Uniquely among integrin ligands, the two IgSF domains of MAdCAM connect to the membrane through a mucin-like stalk of 115 residues. In this respect, MAdCAM resembles selectin ligands (17). Selectins, which are specialized for rolling adhesion in the vasculature and do not mediate firm adhesion, recognize carbohydrate residues displayed on proteins that often consist only of mucin-like regions (4). MAdCAM also contains a disordered, negatively charged loop in domain 2 that functions in adhesion to $\alpha_4\beta_7$ (13), and it has also been proposed to act as a charged antenna that is repelled by the highly negatively charged mucin-like region and helps orient the integrin-binding IgSF domains above the cell surface for recognition (18).

IgSF domain (D) 1 of MAdCAM is especially unusual among integrin IgSF ligands. Both D1 and D2 belong to the I-set, intermediate between IgSF V- and C-set domains in the content of strands on the edges of their two β-sheets. I-set domains differ in having GFC and ABED (I1-set) or GFCC′ and ABE (I2-set) β-sheets, an important distinction because the key integrin-binding site in D1 locates to the β-sandwich edge, which has C and D strands in I1-set and C′ and E strands in I2-set domains. An initial 2.2-Å structure of MAdCAM D1D2 reported that D1 had an I1-set fold like other integrin CAMs (18, 19). As emphasized in a subsequent 1.9 Å structure in the same crystal lattice, the D1 domains of two symmetry-related molecules come together to form a super β-sheet (20). It was further pointed out that the density of the integrin-binding loop was poor and that one edge of the β-strand near the 2-fold symmetry axis at the center of the super sheet should be assigned to the other monomer. Thus, a D strand was reassigned as a C′ strand in the other monomer, changing the topology of the integrin-binding loop and changing D1 from the I1-set to the I2-set, an anomaly among integrin CAMs.

This study was initiated in an attempt to better understand the structure of the key integrin-binding loop of MAdCAM. Structural work on VCAM and ICAMs has continually emphasized that their integrin-binding loops are highly ordered, with a backbone conformation that is highly supported by hydrogen bond networks (11, 12, 19, 21). In the case of ICAMs, the critical integrin-binding Glu residue is even part of β-strand C, as the last residue in the β-strand immediately preceding the CD loop. In VCAM, the crucial Asp is in the CD loop. Furthermore, in the sequence around the integrin-binding Asp/Glu in ICAMs and VCAM, (I/L)(D/E)(T/S), the conserved Thr and Ser residue side chains make hydrogen bonds to backbone to support the conformation of the ligand-binding backbone.

This study shows the opposite for MAdCAM, *i.e.* a highly plastic ligand-binding loop. Over the course of many years and four successive crystal structures, the original crystal form at higher resolution is confirmed to be I2-set and is revealed to likely represent a crystal lattice artifact with two quite different conformations of the integrin-binding loop that coexist in crystals. Complexes of MAdCAM with two function-blocking Fabs, including one in clinical trials, delineate regions important for binding integrins and further views of MAdCAM. These show an I1-set fold for D1 and two different conformations of the integrin-binding loop, depending on whether it is part of the Fab contact site. We discuss the results in the light of observations that integrin $\alpha_4\beta_7$ can mediate both rolling and firm adhesion and EM studies showing that MAdCAM can bind to both open and intermediate conformations of the $\alpha_4\beta_7$ headpiece (16). The unusual flexibility of the integrin-binding loop as shown by its plasticity in four different crystal structures may thus be functionally relevant for MAdCAM's specialization as an integrin ligand that mediates both rolling and firm adhesion.

EXPERIMENTAL PROCEDURES

Wild-type MAdCAM D1D2 used for the 1.7 Å crystal structure was purified from CHO Lec.3.2.8.1 cells and crystallized as described previously (18). RosettaRemodel (22) was used to design MAdCAM mutants with shortened DE loops. No electron density was observed for residues 152–157 in our 1.7-Å structure. We fixed the backbone positions of residues 150 and 158 and enabled the sequence of residue 150 and three more residues to vary (to residues A, F–I, L–N, P–T, V, W, and Y), to complete the hydrogen-bonding pattern of the edge β-strand and allow a two-residue hairpin turn to reconnect back to the structure. After sampling 1000 unique fragment-based trajectories, the top 20 models were visually examined. The 7th ranked and 16th ranked models, with NTGG and PIGG sequences as replacements of residues 150–157, respectively, and an E148Q mutation were chosen for experimental validation. At the time, it was noted that the designs were not ideal, and might have been improved if the position of residue 150 had been allowed to vary; however, this was not tested. The final crystal structure showed a markedly different position for residue Pro-150 than in the original design. In retrospect, retaining the position of residue 150 prevented formation of a β-ribbon continuous with the D and E β-strands; retrospective computation of the structure enabling the position of residue 150 to vary shows a predicted structure more similar to the continuous β-ribbon experimentally observed (data not shown).

Protein Preparation and Crystallization—Residues 1–202 of mature wild type, NTGG, or PIGG mutant human MAdCAM, with the murine immunoglobulin κ chain signal peptide at the N terminus and a His tag HHHHHHA sequence (wild type) or a TEV cleavage site GGENLYFQGG sequence before the His tag (mutants) at the C terminus, were inserted between EcoRI and NotI sites in vector pVLAD6 (23) and confirmed by DNA sequencing. 293S GnTI$^-$ cells (24) were transfected with the BacMAM system (23) and grown in FreeStyle 293 medium (Invitrogen). The PIGG mutant was expressed at higher levels than the NTGG mutant and chosen for further work. Soluble protein was purified by nickel-nitrilotriacetic acid affinity chromatography and then treated with His-tagged TEV protease (only for the PIGG mutant, which contained a TEV cleavage site), followed by re-pass through the nickel-nitrilotriacetic acid column. Flow-through protein was further purified by Mono Q^{TM} 5/50 GL (GE Healthcare) in 20 mM Tris, pH 8.0, with a gradient of 0 to 0.1 M NaCl. Purified protein was either concentrated and screened for crystallization or further complexed with Fabs.

TABLE 1
X-ray diffraction data and refinement

	Wild type	PIGG mutant	PIGG mutant/10G3 Fab	Native/PF00547659 Fab
Wavelength	1.000 Å	1.000 Å	0.979 Å	1.000 Å
Space group	$C222_1$	$P2_12_12_1$	$C2$	$P2_1$
Unit cell (*a*, *b*, *c*)	64.5, 100.0, 69.7 Å	58.3, 69.7, 101.2 Å	317.9, 71.7, 70.6 Å	39.9,112.3,157.9 Å
α, β, γ	90, 90, 90°	90, 90, 90°	90, 93.3, 90°	90, 89.9, 90°
Resolution	21–1.7 Å	38–1.4 Å	50–2.9 Å	48–2.3 Å
Reflections (total/unique)	106364/23698	558714/81325	128467/35879	195317/59513
Completeness	94.6% (72.8%)[a]	99.2% (94.3%)[a]	100% (100%)[a]	96.1% (94.4%)[a]
$I/\sigma(I)$	17.9 (2.6)[a]	16.1 (1.6)[a]	10.6 (2.0)[a]	14.3 (4.8)[a]
R_{merge}[b]	6.1% (36.4%)[a]	6.7% (121.0%)[a]	12.6% (65.6%)[a]	6.5% (26.8%)[a]
Refinement				
R_{cryst}[c]	17.1%	14.3%	20.0%	15.4%
R_{work}[d]	21.4%	17.9%	25.3%	20.8%
r.m.s.d. bond length	0.009 Å	0.009 Å	0.004 Å	0.010 Å
r.m.s.d. angles	1.341°	1.358°	0.916°	1.506°
Examples/asymmetric unit	1	2	2	2
Ramachandran[e] (% favored/allowed/outlier)	99/1/0	99/1 /0	96.2/3.7/0.1	97.0/2.8/0.2
Molprobity percentiles[e] Clashscore/geometry	93/91	94/89	100/100	96/96
Protein Data Bank code	4HD9	4HBQ	4HC1	4HCR

[a] Numbers correspond to the last resolution shell.
[b] $R_{merge} = \Sigma_h \Sigma_i |I_i(h) - \langle I(h)\rangle| / \Sigma_h \Sigma_i I_i(h)$, where $I_i(h)$ and $I(h)$ are the ith and mean measurement of the intensity of reflection, h.
[c] $R_{work} = \Sigma_h (||F_{obs}(h)| - |F_{calc}(h)||) / \Sigma |F_{obs}(h)|$, where $F_{obs}(h)$ and $F_{calc}(h)$ are the observed and calculated structure factors, respectively.
[d] R_{free} is the R-factor for a selected subset of the reflections that are not included in refinement calculation.
[e] Data were determined with MolProbity (37).

The 10G3 hybridoma was kindly provided by M. Briskin (LeukoSite, Cambridge, MA) (13). The 10G3 antibody was purified by a protein G column from culture supernatant. Xenomouse™ monoclonal antibody PF-547659 was from Pfizer, Cambridge, MA (25). Fabs were generated by soluble papain with a weight ratio of 1:100 (enzyme/antibody) in phosphate-buffered saline, pH 7.0, with 1 mM EDTA, 10 mM cysteine at 37 °C for 12 h. Undigested IgG and Fc fragments were removed by passage through a protein A column. Fabs were further purified by Mono Q, from which they eluted in the flow-through in 10 mM Tris, pH 8.5, followed by gel filtration on Superdex 75. Purified MAdCAM and PIGG mutant were incubated with PF-547659 Fab or 10G3 Fab, respectively, at a 1:2 molar ratio at room temperature for half an hour. The complex was then separated by gel filtration on Superdex 200 in Tris-buffered saline, pH 7.5, and concentrated to 15–20 mg/ml for crystal screening.

Crystals of the MAdCAM PIGG mutant were from 0.1 M Tris, pH 8.5, 0.2 M $(NH_4)_2SO_4$, 12% polyethylene glycol (PEG) 8000. Crystals of MAdCAM PIGG·10G3 Fab complex were from 0.1 M Tris, pH 7.0, 10% (w/v) PEG monomethyl ether (PEGMME) 2000. Crystals of MAdCAM·PF-547659 Fab complex were obtained from 0.1 M citrate, pH 6.0, 18% (w/v) PEG 3350, 12% (w/v) myo-inositol. For cryoprotection, crystals were transferred into reservoir solution with a 1.2-fold higher precipitant concentration, also containing 20% glycerol, and then flash-frozen at 100 K. Data sets were collected at Advanced Photon Source beamlines ID23 or ID24. Diffraction data were processed with XDS (26) or HKL2000 (Table 1) (27).

Structure Determination and Refinement—All four structures were determined by molecular replacement with PHASER (28). For the MAdCAM·Fab complex, we searched for Fab first and then MAdCAM. Solutions from molecular replacement were subjected to iterative cycles of model building in COOT (29), refinement using REFMAC (30) or PHENIX (31), and validation with MOLPROBITY (32).

In the 1.4-Å $P2_12_12_1$ structure, the second conformation of the integrin-binding loop was first traced by XPLEO (32) and rebuilt manually in COOT, and it was then used to guide building of two conformations in the 1.7-Å $C222_1$ structure.

During refinement of the MAdCAM·10G3 Fab complex, side chain density in the A β-strand but not in the A′ β-strand in D1 of MAdCAM was discrepant, and a gap between the A and A′ β-strands was present with unexplained nearby density. No such gap was found in MAdCAM in any of the other crystal structures characterized here. We found continuous density extending from the C-terminal end of another MAdCAM molecule in the crystal lattice into the A β-strand. The densities were well explained, and R_{free} dropped, when we built a GGENLYFQ sequence remaining at the C terminus of MAdCAM after TEV cleavage as continuing from the end of one MAdCAM molecule into the A β-strand of another MAdCAM molecule. In other words, residual residues remaining after TEV cleavage displaced native MAdCAM residues in the A β-strand in D1 of a neighboring molecule in the lattice, and this occurred only in the 10G3 Fab complex structure.

RESULTS

Wild-type and PIGG Mutant Crystal Forms—Crystals similar to those solved at 2.2 Å with in-house diffraction (18) gave synchrotron diffraction to 1.7 Å (Table 1 and Fig. 1*A*). Initial refinement confirmed the conclusions from the 1.9-Å structure (20) that D1 of MAdCAM crystallized as an I2-set domain and that density was poor for the integrin-binding loop. However, we were dissatisfied that regions with clearly discernable density could not be well fit with atomic models. The difficult regions to model corresponded to residues 40–47 containing the putative integrin-binding Asp-42.

With the hope of obtaining a different crystal lattice, we designed truncations of the disordered charged antenna DE loop in D2. We used a precursor of Rosetta Remodel (22) to design four-residue sequences to substitute for an EEEPQGDE

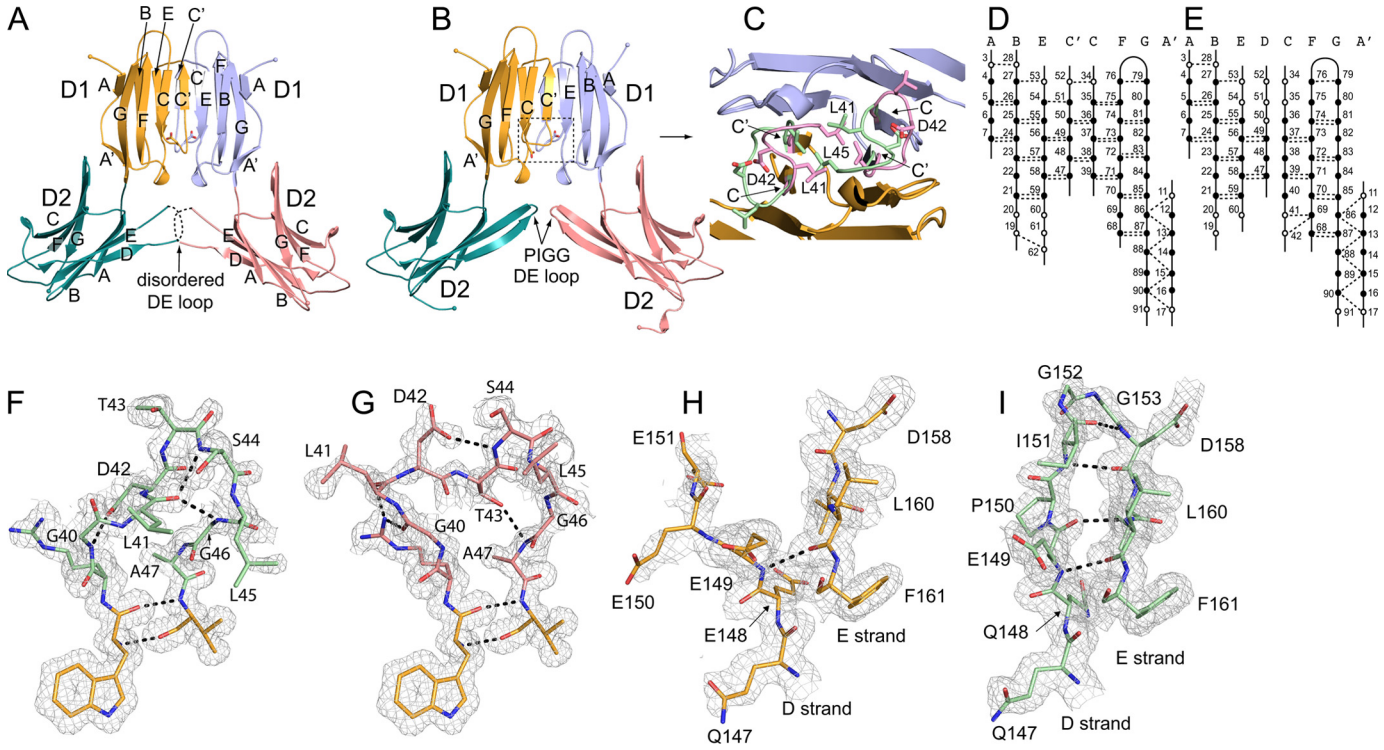

FIGURE 1. **Crystal structures of domains 1 and 2 of MAdCAM.** *A* and *B*, overall structure of wild-type (*A*) and PIGG mutant (*B*) MAdCAM D1D2. The super β-sheet in D1 is formed by two symmetry-related molecules (*A*) or two distinct molecules related by pseudosymmetry (*B*). For simplicity, only one CC′ loop conformation is shown in *A* and *B*. *C*, two conformations of the integrin-binding CC′ loop in the PIGG mutant. Conformations A and B are in *pink* and *pale green*, respectively. Leu-41, Leu-45, and Asp-42 side chains are shown as *sticks*. *D* and *E*, β-sheet hydrogen bonds in D1. The super β-sheet in the 1.4-Å structure with a C′ β-strand (*D*) is contrasted with the two separate β-sheets in D1 in the complex with Fab PF-547659 (*E*). Residues in β-sheet framework and loops are shown in *solid* and *open circles*, respectively. Backbone hydrogen bonds are *dashed lines*. *F* and *G*, electron density around conformation A (*F*) and B (*G*) of the integrin-binding CC′ loop is shown in the PIGG mutant 1.4 Å structure. $2F_o–F_c$ 0.7 σ density is carved within 1.4 Å of the illustrated atoms. *H* and *I*, DE loop in D2. Electron density is shown neighboring the disordered DE loop in the wild-type MAdCAM 1.7 Å structure (*H*) and around the ordered DE loop in the PIGG mutant 1.4 Å structure (*I*). $2F_o–F_c$ σ density is carved within 1.7 Å of the illustrated atoms.

eight-residue sequence that was largely disordered in the 1.7-Å structure. A mutant with a four-residue PIGG sequence replacement and an E148Q replacement crystallized under many conditions, including with either polyethylene glycol (PEG) or salt as precipitant. However, all conditions gave the same space group and similar unit cell dimensions.

The MAdCAM D1D2 PIGG mutant diffracted to 1.4 Å in space group $P2_12_12_1$ (Table 1 and Fig. 1*B*). However, the interactions between neighboring molecules in the lattice were almost identical to those in the wild-type $C222_1$ crystal form, with the same D1 super β-sheet (Fig. 1, *B* and *D*). The super β-sheet is formed by two independent molecules in the asymmetric unit related by a 2-fold pseudosymmetry axis in the $P2_12_12_1$ crystal form (Fig. 1*B*), compared with identical molecules related by 2-fold crystallographic symmetry in the $C222_1$ crystal form (Fig. 1*A*). The overall structure of the PIGG mutant is very similar to that of wild-type MAdCAM, except a highly ordered mutant DE loop in D2 (Fig. 1, *B* and *I*) substitutes for the largely disordered wild-type DE loop (Fig. 1, *A* and *H*).

The 1.4-Å structure revealed evidence for two conformations of the integrin-binding loop between residues 40 and 47; however, it was difficult to build both conformations manually. Inverse kinematics can automate building of missing loops into proteins guided by the electron density, including loops present in multiple backbone conformations at resolutions of 1.8 Å or higher (33). This method readily found two alternative conformations for residues 40–47, which, after some manual rebuilding, fit the electron density well (Fig. 1, *C*, *F*, and *G*). One alternative CC′ loop conformation was stabilized by three internal hydrogen bonds (Fig. 1*F*) and further external hydrogen bonds (supplemental Fig. S1*A*). The other alternative conformation was stabilized by a similar number but completely different set of hydrogen bonds (Fig. 1*G* and supplemental Fig. S1*B*).

The electron density of the 1.7-Å $C222_1$ crystal form showed strong evidence for two similar, alternative backbone conformations of the CC′ loop. The 1.4-Å $P2_12_12_1$ structure was used to guide building of these loops in the 1.7-Å structure. Alternative conformations in both structures were also built for residues Arg-60 and Asn-61 in the EF loop that interacts with alternative conformations of the neighboring CC′ loop. In the 1.4-Å structure, the *N*-acetylglucosamine residue attached to Asn-61 was visible in two alternative conformations in chain B but was disordered in chain A.

The final R_{work} and R_{free} are 14.3 and 17.8% (1.4-Å structure) and 17.1 and 21.4% (1.7-Å structure). The geometries are excellent, with MolProbity (32) reporting no Ramachandran outliers in either structure (Table 1) compared with 10.1 and 2.5% outliers in the previous 2.2- and 1.9-Å structures, respectively. The previously reported MAdCAM structures (18, 20) have almost identical unit cell dimensions (within 1 Å) and the same $C222_1$ space group as our 1.7 Å structure. Similar alternative backbone conformations within the previous structures are consistent

with reported poor density for the CC′ loop in the 1.9-Å structure (20); the path built for the single CC′ loop conformation in the 1.9 Å structure is intermediate between the two built in our 1.7-Å structure.

The total solvent-accessible surface area buried by the formation of the super β-sheet in D1 is ~2100 Å^2. This lattice contact is unusually large in size (34) and is sufficient to perturb the interacting regions away from their native structure. Notably, the CC′ loop with two conformations lies adjacent to C′, which hydrogen bonds to the E strand of the other monomer across the super β-sheet interface (Fig. 1*D*). Furthermore, the two reciprocal C′-E and E-C′ β-sheet interfaces squeeze the two CC′ loops tightly together at the super β-sheet interface (Fig. 1*C*). One of the two alternative loop conformations comes close to the 2-fold dyad axis. Close to this 2-fold axis severe clashes exist between Leu-41 from one molecule and Leu-45 from another molecule in the $P2_12_12_1$ structure (Fig. 1*C*) and between the symmetry-related Leu-45 side chains in the $C222_1$ structure (supplemental Fig. S1*C*). Thus, at each dimer interface within the crystal, one monomer must have the dyad-proximal alternative conformation of the CC′ loop, and the other monomer must have the complementary, dyad-distal alternative conformation.

The differences between the two conformations of the CC′ loop are extreme (Fig. 1, *C*, *F*, and *G*). A radical divergence begins at Gly-40, with a backbone flip as often seen at Gly residues. The two alternative backbones then run in almost opposite directions, diverging 6 Å at the Leu-41 Cα atoms. Distances between alternative Cα atoms are as follows: 4.5 Å at Asp-42; 5 Å at Thr-43 and Ser-44; 4 Å at Leu-45; and 1.5 Å at Gly-46, before returning to close proximity of 0.5 Å at the Cα of Ala-47. The importance of Gly-40 and Gly-46 in backbone divergence is a topic under the "Discussion."

Two Fab Complex Crystal Forms—The above 1.4 and 1.7 Å crystal structures demonstrated that residues 40–46, bearing the key integrin-binding loop in MAdCAM, are capable of remarkable backbone plasticity. However, this plasticity was seen in the context of a large, super β-sheet lattice contact that we worried might cause the structure to be artifactual in the region of lattice contacts. Fab complexes would necessarily have completely different crystal lattices and would provide insights into mechanism of inhibition by antibodies of MAdCAM function. We therefore determined MAdCAM co-crystal structures with two different Fabs.

We first describe the complex of 10G3 Fab (35) and PIGG mutant MAdCAM. This structure at 2.9 Å resolution was refined to R_{work} of 20.0% and R_{free} of 25.3% and contains two complexes per asymmetric unit (Table 1). There is no D1 super β-sheet in this crystal form.

Remarkably, D1 of MAdCAM in this novel crystal form and in the second Fab complex described below assumes the I1-set fold, *i.e.* instead of forming a C′ strand in a super β-sheet interface (Fig. 1*D*), the residues shift over to the opposite β-sheet to form a D-strand in an ABED β-sheet (Figs. 1*E* and 2*A*). The 10G3 Fab contacts solely the D1 domain of MAdCAM and buries a total solvent-accessible surface area of 1600 Å^2. MAdCAM residue Leu-45 binds in a tyrosine-containing pocket created by Fab H chain CDR1, CDR2, and CDR3 and L chain CDR3 loops

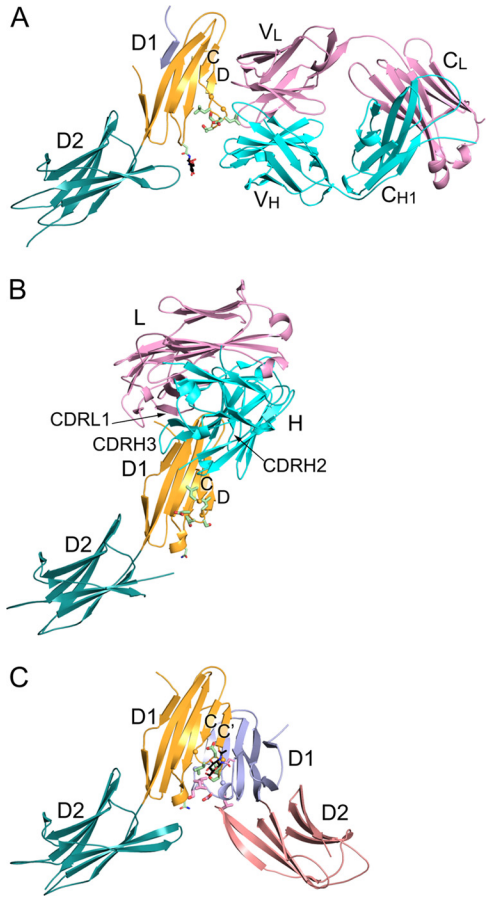

FIGURE 2. **Overview of MAdCAM Fab complex structures and comparison with MAdCAM alone.** *A,* 10G3 Fab complex with PIGG mutant MAdCAM. *B*, PF-547659 Fab complex with wild-type MAdCAM. *C,* comparison with PIGG mutant MAdCAM D1D2 alone. The structures are in identical orientations after superposition on the MAdCAM molecule shown with *orange* D1 and *teal* D2. The other MAdCAM molecule in *C* has *light blue* D1 and *pink* D2. Fab H and L chains are *cyan* and *pink*, respectively. MAdCAM side chains in the integrin-binding loop and *N*-glycosylation site residue Asn-61 are shown as *green stick*, and the glycan as *black* carbons. MAdCAM Gly residues 40 and 46 are *orange* Cα *spheres*. *A*, D1 β-strand shown in *light blue* is contributed by a lattice contact that displaces the native A β-strand.

(Fig. 3*A*). The side chain and main chain of H chain CDR3 residue Asp-101 participate in multiple hydrogen bonds to the main chain of D1 residues 44, 46, and 47. Residues of the D1 CD loop including Asp-42 form side chain and main chain contacts with the H chain. Residues in the C and D strands of MAdCAM D1 form further hydrogen bonds and van der Waals interactions with the L chain (Fig. 3*A*). Because of the intimate interaction of the Fab with the CD loop of MAdCAM D1, including its backbone, an influence of the Fab on D1 CD loop conformation could not be ruled out.

A complex of wild-type MAdCAM D1D2 and Fab PF-547659 crystallized in space group $P2_1$. The structure with two complexes in an asymmetric unit was refined to a resolution of 2.3 Å with R_{work} of 15.4 and R_{free} of 20.8% (Table 1). Again, there is no super β-sheet in the lattice, and D1 adopts an I1-set fold (Fig. 2*B*). Fab PF-547659 binds to loops in the N-terminal tip of D1 of MAdCAM and to neighboring portions of the CFG β-sheet (Fig. 2*B*) and buries a total of 2000 Å^2. The H2, H3, and L1 CDR loops are unusually long and form a crevice in which the tip of D1 is buried (Fig. 2*B*). At the tip of D1, its N-terminal α-amino

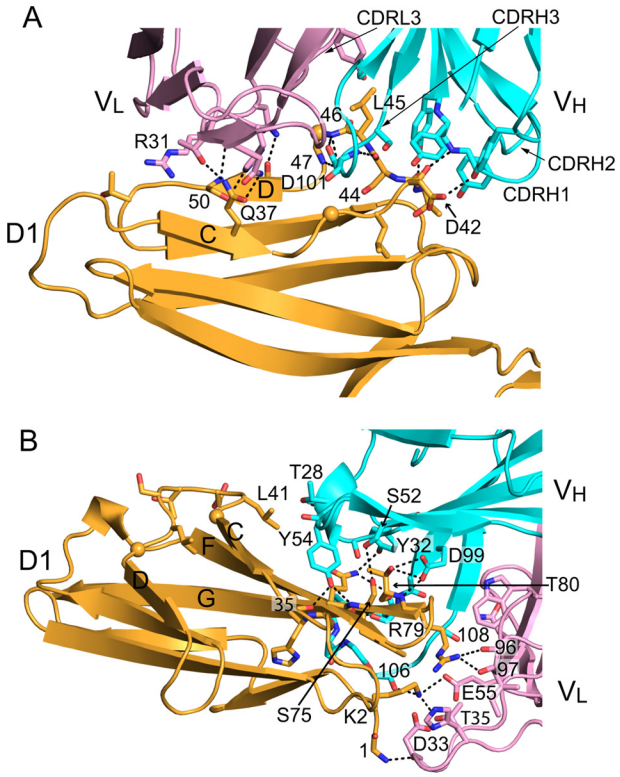

FIGURE 3. **MAdCAM-Fab interfaces.** *A,* MAdCAM complex with 10G3 Fab. *B*, MAdCAM complex with PF-547659 Fab. Heavy chain is *cyan*; light chain is *pink,* and MAdCAM D1 is *orange*. Side chains and main chain atoms in the interfaces and the integrin binding loop of MAdCAM are in *stick*. MAdCAM Gly residues 40 and 46 have Cα spheres. *Dashed lines* show hydrogen bonds across the interfaces.

group and Lys-2 and Arg-79 side chains interact with an oxygen-rich Fab pocket containing Asp, Glu, and Thr side chains and four backbone carbonyl groups (Fig. 3*B*). The side chain of H chain residue Glu-99 makes hydrogen bonds to the side chain and backbone of Thr-80 in MAdCAM D1 β-strand G. Extending across the CFG β-sheet, H chain CDR2 residues Ser-52 and Tyr-54 interact with β-strand F residue Ser-75 and BC loop residue 35 (Fig. 3*B*). On the very periphery of the interface, the side chain of Thr-28 in the H chain CDR1 loop makes a van der Waals contact with the side chain of MAdCAM residue Leu-41. Notably, there are no other contacts with the integrin-binding CD loop.

D1-D2 Interface and the DE Loop in D2—The interface between D1 and D2 in MAdCAM includes the DE loop in D2, which is important in integrin binding (Fig. 4, *A* and *B*). Our structures include three examples of MAdCAM with the native sequence of the DE loop in D2, one in the 1.7 Å structure and two in the 2.3 Å complex with PF-547659. Prior to the disordered portion of this loop, a stretch of four consecutive Glu residues, 148–151, is visible in the 1.7Å structure (Fig. 4*A*), and two of these, residues 148 and 149, are visible in the Fab complex (Fig. 4*B*). The orientation of these residues differs in all three structures, consistent with lack of density for residues 152–157 or 150–157. However, after the disordered residues, Asp-158, Val-159, and Leu-160 have a similar conformation in all three structures (Fig. 4, *A* and *B*). Furthermore, the side chain of Asp-158 hydrogen bonds to the backbone of residue Leu-64 at the beginning of a 3_{10} helix in the EF loop of D1 (Fig. 4, *A* and *B*). This hydrogen bond contributes to the D1-D2 interface and is conserved among all three examples of wild-type MAdCAM. Many hydrophobic residues, including Leu-160, contribute to the D1-D2 interface (Fig. 4, *A* and *B*), to ensure an optimal orientation between these domains for binding to $\alpha_4\beta_7$, as further discussed below.

DISCUSSION

This study changes structural understanding of MAdCAM in several important respects. Although two previous studies provided different interpretations of the chain trace in D1, they were limited to a single crystal form with one molecule per asymmetric unit. Our study extends this crystal form to a higher 1.7 Å resolution and a related crystal form to 1.4 Å and re-interprets the chain trace of the integrin-binding loop as consisting of two markedly different alternative conformations. But more importantly, we have obtained independent views of MAdCAM in quite different crystal lattices that demonstrate a different I1-set fold for D1. Multiple conformations for the integrin-binding loop are revealed in both I1-set and I2-set D1 folds. Because there were two molecules per asymmetric unit in the three latter crystal forms, we now have a total of seven views of MAdCAM in crystals. Here we discuss the following: 1) the physiological significance of the I1-set D1 fold; 2) the specializations in the D1-D2 interface in MAdCAM that correlate with less variation in the D1-D2 interface in MAdCAM than in VCAM; 3) the contrast between the structure of the integrin-binding loops in MAdCAM and VCAM; 4) the interpretation of previous mutational studies and mechanism of antibody inhibition in light of the new structural information; and finally 5) the implication of the flexible DE loop in D2 and flexible integrin-binding loop in D1 for ability of $\alpha_4\beta_7$ to mediate both rolling and firm adhesion.

The super β-sheet seen in D1 in the previous $C222_1$ crystal form and the new $P2_12_12_1$ form is likely to be a crystal artifact. The fragment containing two IgSF domains of MAdCAM does not dimerize at high concentrations in solution (20). There is no evidence for MAdCAM dimerization on cell surfaces. Furthermore, dimerization on cell surfaces would be inhibited by electrostatic repulsion between the 115-residue mucin-like domain in each MAdCAM monomer, with many sialylated *O*-linked glycans and high content of Asp and Glu (18), as well as between the highly negatively charged DE loop in D2. Dimerization at the super β-sheet interface largely buries the integrin-binding loop in D1 and also occludes the functionally important DE loop in D2 (Fig. 1, *A* and *B*). The large 2100-Å^2 interface is greatly above the average of 570 Å^2 and above the 99th percentile of 1600 Å^2 for lattice interactions (34) and is extending into the range of interfaces of 2000 Å^2 or larger where conformational change is often associated with protein-protein binding (36). In contrast, the edge β-strands in the I1-set conformation of D1 seen here did not participate in any significant lattice contacts, and were involved in contacts with Fab in only one of the two Fab complexes. Each antibody studied here was selected for binding to MAdCAM on cell surfaces and for complete inhibition of binding to integrin $\alpha_4\beta_7$ (25, 35). Therefore, we conclude that the I1-set conformation of MAdCAM D1 is

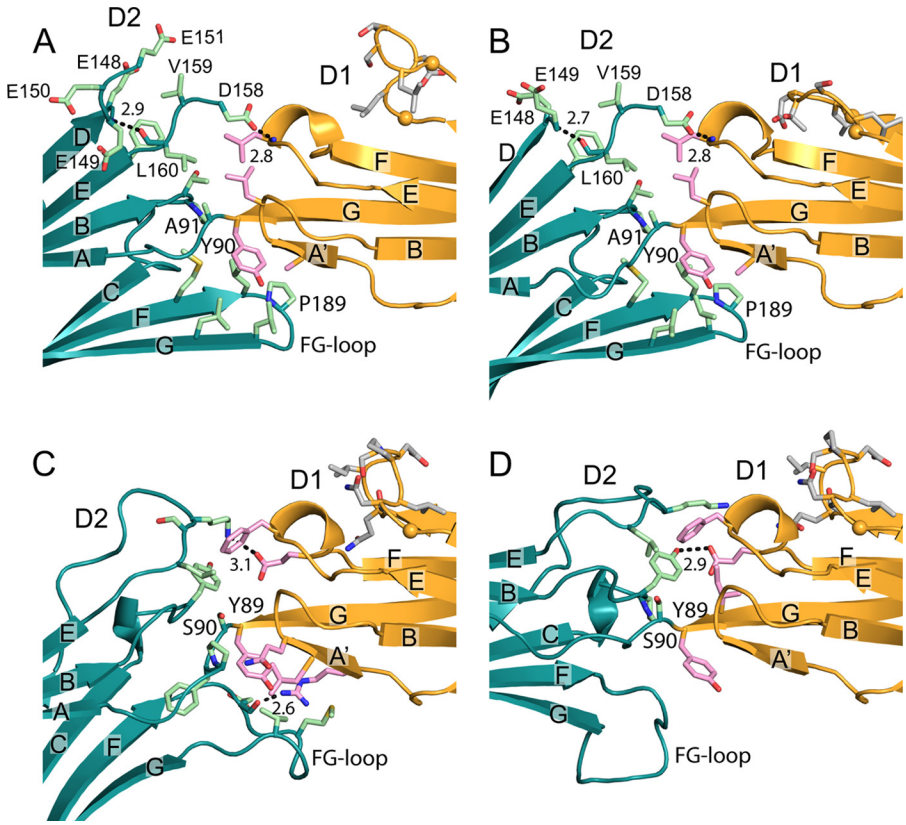

FIGURE 4. **Interface between D1 and D2 in MAdCAM and VCAM.** *A* and *B* show the most dissimilar native MAdCAM interfaces in the 1.7-Å structure (*A*) and chain B in complex with PF-547659 (*B*). *C* and *D* show the most dissimilar VCAM interfaces in chain A of Protein Data Bank code 1VCA (11) (*C*), and chain B of Protein Data Bank code 1VSC (12) (*D*). Interface side chains have *green* (D2) and *pink* (D1) carbons. Hydrogen bonds across interfaces and are shown as *dashed lines* together with their distances in Å. Side chains in integrin-binding CD loops have *silver* carbons.

the predominant, biologically relevant conformation on cell surfaces. However, we cannot exclude dynamic equilibrium with a low proportion of MAdCAM molecules with an I2-set D1 IgSF fold.

It is common for significant flexibility to be seen between tandem IgSF domains, as previously exemplified in ICAM-1 and VCAM (19). Tyr or Phe is conserved as the last residue in the IgSF domains of integrin ligands, and flexibility between domains is accommodated by their interaction with hydrophobic residues in the tandem domain (19). Our results demonstrate less variation in D1/D2 orientation among MAdCAM molecules than among VCAM molecules. The three examples of wild-type MAdCAM molecules in crystal lattices differ by 5 ± 3° (mean ± S.D.) and 1–9° (range) in orientation. The PIGG mutation is at the D1-D2 interface; when PIGG mutant molecules are included, the seven examples of MAdCAM molecules differ by 10 ± 5° (1–20°). Among five examples of VCAM molecules seen in crystals (11, 12, 21), variation in D1/D2 orientation is 19 ± 8° (7–35°). The interfaces with greatest variation among wild-type MAdCAM and VCAM structures are shown in Fig. 4. In MAdCAM, a hydrogen bond links the DE loop of D2 to the EF loop in D1 (Fig. 4, *A* and *B*). Nearby, the Leu and Thr residues in D2 and the Leu residues in D1 form a hydrophobic interface (Fig. 4, *A* and *B*). The last residue in D1 and the first residue in D2, Tyr-90 and Ala-91, each have two main chain hydrogen bonds within their domains, limiting interdomain movement, as is also true for the homologous Tyr-89 and Ser-90 residues in VCAM (Fig. 4, *C* and *D*). Tyr-90 in D1 of MAdCAM interacts with four hydrophobic residues in the F and G β-strands and FG loop of D2 (Fig. 4, *A* and *B*). Pro-189 also interacts with D1 hydrophobic residues. By contrast, the FG loop in VCAM is much more variable in conformation among crystal structures (Fig. 4, *C* and *D*). Both D1 and D2 of MAdCAM make important contributions to integrin binding, and a pre-formed orientation between these domains may be important to the rapid binding kinetics required for $\alpha_4\beta_7$ to mediate rolling adhesion.

Compared with VCAM, the integrin-binding loop in MAdCAM is highly flexible. We found two very distinct alternative loop conformations in the I2-set fold and two distinct conformations in the I1-set fold bound to two different Fab. Now that we found that both MAdCAM and VCAM have I1-set folds, meaningful structure-based sequence alignment is possible (supplemental Fig. S2). The CD loop is two residues longer in VCAM than MAdCAM (Fig. 5*A*). Furthermore, their integrin-binding LDT and IDS motifs do not align either in sequence (Fig. 5*A*) or in structure (supplemental Fig. S2).

In VCAM, Thr-37 nucleates a network of hydrogen bonds that stabilizes a β-hairpin type I turn with multiple hydrogen bonds to the Ile-39, Asp-40, and Ser-41 (IDS) motif (Fig. 5*B*). The Thr-37 side chain forms two hydrogen bonds to the backbones of Ile-39 and Ser-41, one to the side chain of Ser-41 and a main chain-main chain Thr-37 to Asp-40 type I β-turn hydrogen bond. This places Leu-39 and Asp-40 in a highly con-

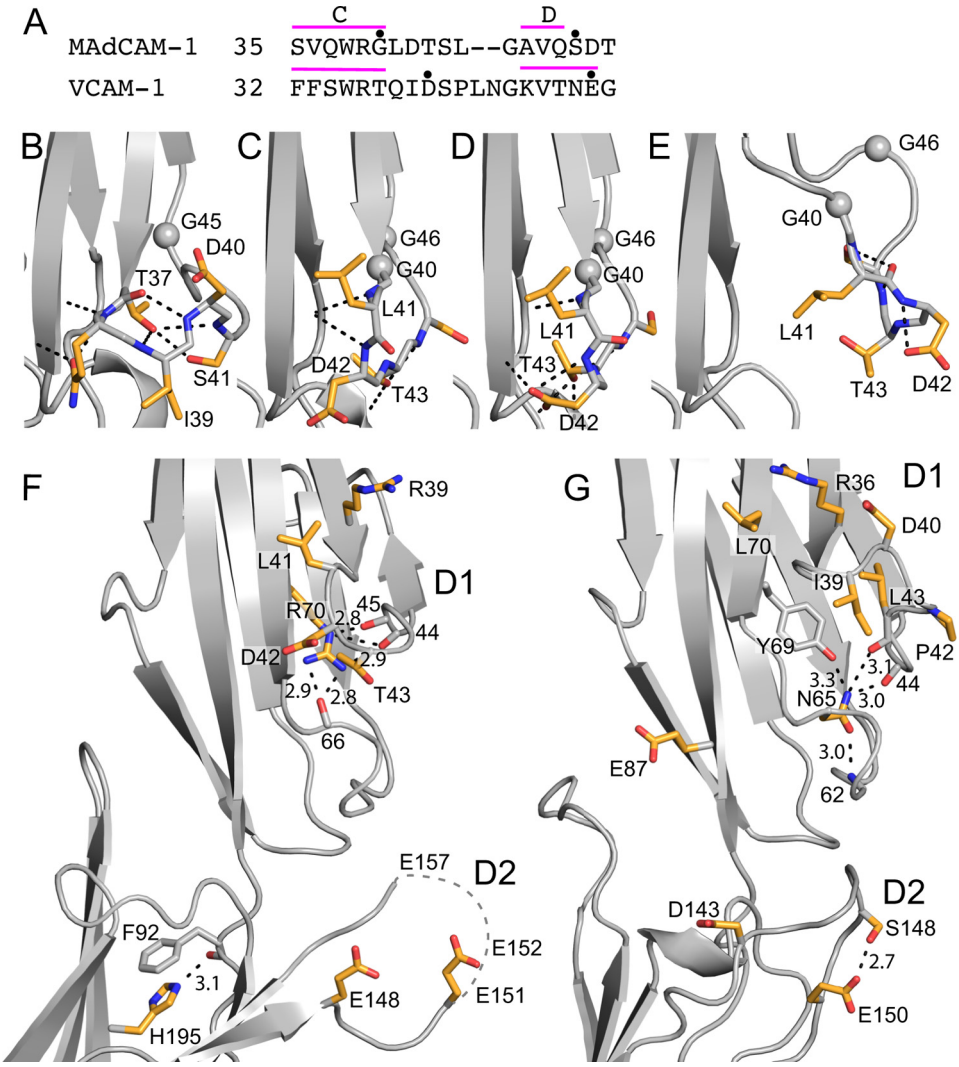

FIGURE 5. **Integrin-binding residues in MAdCAM and VCAM.** *A,* sequence alignment between MAdCAM and VCAM at the integrin-binding CD loop. *β*-Strands in MAdCAM complex with PF-547659 Fab and in VCAM are *overlined*, and decadal residues are *dotted*. *B–E,* hydrogen bonds in first portion of the CD loop in VCAM (*B*) and MAdCAM (*C–E*). MAdCAM molecules are from the PF-547659 Fab complex (*C* and *D*) and 10G3 Fab complex (*E*). *B–E* are in identical orientations after superposition on D1. Side chains of residues 37–41 of VCAM and 40–43 of MAdCAM are shown as *sticks* with *orange* carbons, and all hydrogen bonds formed by these residues are *dashed black lines*. *F* and *G,* functionally important side chains of MAdCAM (*F*) and VCAM (*G*). Molecules are in identical orientations after superposition on D1. Residues mutation that decreases integrin binding by 75% or more are shown with side chains with *gold* carbons, and side chains or main chain atoms of important nearby interacting residues are shown with *silver* carbons. Hydrogen bonds formed by side chains of mutationally identified residues are shown as *black dashed lines* together with their distances in Å to one decimal. Numbers without decimals label residues that participate in backbone hydrogen bonds. The MAdCAM molecule is a chimera of the complex with PF-547659 (residues 1–139 and 169–199) and the 1.7 Å structure (residues 140–168), which includes more DE loop residues in D2. Mutationally important residues in the disordered portion of the DE loop are shown with labels in *F*.

strained tight *β*-turn, and all five examples of VCAM crystal structures share this same hydrogen bond pattern (11, 12, 21).

The hydrogen bond pattern in the equivalent region of MAdCAM is not conserved between the two Fab complex structures, and even the two different examples in complex with PF-547659 Fab share only one hydrogen bond (Fig. 5, *C–E*). In place of the highly stabilizing Thr-37 in VCAM, MAdCAM has Gly-40 (Fig. 5, *A* and *C–E*). Not only does Gly lack the potential to form the three key side chain hydrogen bonds formed by Thr-37 of VCAM, its main chain is the most flexible of any amino acid. The marked difference in two alternative CC′ loop conformations in the I2-set fold of MAdCAM D1 begins with a backbone flip at Gly-40. Moreover, the marked variation in CD-loop conformation in the I1-set fold of MAdCAM with two different Fabs begins with Gly-40 and ends with Gly-46 (Fig. 5, *D* and *E*).

Thus, the substitution of Gly-40 in MAdCAM for Thr-37 in VCAM and the quite different CD loop sequences in MAdCAM and VCAM (Fig. 5*A*) have profound consequences for the conformation and flexibility of the integrin-binding loop. Results with VCAM chimeras are consistent with the importance of Thr-37 and the length of the integrin-binding loop in VCAM (15). Superior adhesion to $\alpha_4\beta_1$ was given when Thr-37 was retained, and the MAdCAM sequence GLDTS was substituted for QIDSP in VCAM. In contrast, elimination of Thr-37 and shortening the loop by substituting the MAdCAM sequence GLDTSL for TQIDSPLN in VCAM abolished adhesion to $\alpha_4\beta_1$ (15).

Previous mutational studies on MAdCAM (13, 37) require re-evaluation in light of the I1-set fold in D1 described here. Mutations decreasing $\alpha_4\beta_7$-dependent adhesion by 75% or more are shown with gold side chains in Fig. 5*F*. Important MAdCAM residues Arg-39 in the C β-strand and Leu-41, Asp-42, and Thr-43 in the CD loop are surface-exposed in D1. Similarly, Glu-148 and Glu-151 in the DE-loop of D2, as well as Glu-152 and Glu-157 in the disordered portion of this loop, are surface-exposed and nearby. His-195 in D2 is not surface-exposed but may be important to stabilize the D1-D2 interface by making a hydrogen bond and π-cation, aromatic stacking interaction with Phe-92 (Fig. 5*F*). Deletion of residues 152–158 in the DE loop in D2 of MAdCAM almost completely abolishes $\alpha_4\beta_7$-dependent accumulation of rollingly adherent cells on MAdCAM-1 in shear flow in Ca^{2+} and Mg^{2+}, and it only partially inhibits accumulation of firmly adherent cells in Mn^{2+} (46). Similarly, replacement of residues, with the PIGG mutant studied here abolished MAdCAM-1 function in Ca^{2+} and Mg^{2+} and had little effect in Mn^{2+}.[3]

Residues on VCAM shown to be important in binding to integrins $\alpha_4\beta_1$ and $\alpha_4\beta_7$ (15, 38) are similarly shown with gold side chains in Fig. 5*G*. Arg-36 in the C β-strand and Ile-39, Asp-40, Pro-42, and Leu-43 in the CD-loop are surface-exposed. The binding interface extends to Leu-70 in the F β-strand and Glu-87 in the G β-strand in D1. Furthermore, Asp-143, Ser-148, and Glu-150 in the C′E loop of VCAM D2 contribute to the binding interface (Fig. 5*G*) analogously to the acidic residues in the equivalent DE loop of MAdCAM D2 (Fig. 5*F*). Overall, MAdCAM and VCAM show similar footprints for α_4 integrin binding (Fig. 5, *F* and *G*).

Buried residues in D1 that are mutationally important for binding α_4 integrins are Arg-70 in MAdCAM (Fig. 5*F*) (13) and Asn-65 in VCAM (Fig. 5*G*) (38). In the PF-547659 Fab complex, which likely has a more physiological CD loop because this loop is outside the Fab-binding site, the Arg-70 side chain nucleates a hydrogen bond network in MAdCAM that is identical to that nucleated by the Asn-65 side chain in VCAM (Fig. 5, *F* and *G*). In other words, these side chains hydrogen bond to equivalent backbone carbonyl groups in the CD loops of MAdCAM (residues 44 and 45) and VCAM (residues 43 and 44), placing this portion of the CD loop in very similar positions in the two molecules. Moreover, in VCAM Asn-65 hydrogen bonds to Tyr-69 (not yet tested mutationally), which is homologous to Arg-70 in MAdCAM (Fig. 5, *F* and *G*). Conversely, in MAdCAM Arg-70 hydrogen bonds to the carbonyl group of residue 66, which corresponds to Asn-65 in VCAM.

Because MAdCAM and VCAM both bind to integrin $\alpha_4\beta_7$, it is likely that in integrin binding the flexible CD loop of MAdCAM adopts a conformation similar to the rigid CD loop of VCAM. The PF-547659 Fab complex with MAdCAM has a CD loop closest in conformation to that of VCAM (Fig. 5, *C* and *D*). However, to more closely mimic the VCAM conformation, the portion of the CD loop bearing MAdCAM residues Leu-41, Asp-42, and Thr-43 would need to bend toward the N-terminal end of D1, which would bring Asp-42 toward Arg-39 and fold Leu-41 over Arg-70 (Fig. 5*F*). This would place Asp-42 and Leu-41 in MAdCAM in positions analogous to Asp-40 and Ile-39 in VCAM. Because residues 41–43 in MAdCAM are outside the hydrogen bond network secured by Arg-70, this conformational change should be facile.

The flexibility of the CD loop in D1 and adjacent DE loop in D2 of MAdCAM raise the interesting possibility of a "bait-and-switch" mechanism for integrin binding. In the first step in rolling adhesion, a leukocyte free in flow tethers to the endothelium. To support rapid bond formation in tethering, as well as in bond formation to downstream sites during lymphocyte rolling, it is thought that high k_{on} rates are required (4). A basic surface on $\alpha_4\beta_7$ surrounding the metal ion-dependent adhesion site (MIDAS), including the specificity-determining loop of β_7, has been identified (16). Electrostatic forces operate over longer distances than van der Waals and hydrogen bonds and are commonly used in the vasculature to obtain fast on-rates, for example in the clotting cascade (39). The mutationally important Glu residues in the D2 DE loop of MAdCAM may act as the bait for initial interaction with the basic patch and possibly even the MIDAS of $\alpha_4\beta_7$. After initial formation of a desolvated protein·protein complex, subsequent protein motions may result in switching to a conformation with Asp-42 of D1 bound to the MIDAS, and the DE loop of D2 may also become ordered to interact with the basic patch of $\alpha_4\beta_7$.

Another interesting consequence of the flexibility of the D1 CD loop is its compatibility with two conformations of the $\alpha_4\beta_7$ integrin. It is well established by mutation of the β_7 βI domain and use of different divalent cations that $\alpha_4\beta_7$ has two discrete states, one of which mediates rolling adhesion and a second that mediates firm (high affinity) adhesion (6, 40). Remarkably, EM of $\alpha_4\beta_7$ demonstrates three conformational states (16). In the absence of ligand, $\alpha_4\beta_7$ has predominantly a closed headpiece. MAdCAM binding induces an intermediate conformation of the headpiece. Addition of Mn^{2+} converts MAdCAM·$\alpha_4\beta_7$ complexes largely to the open headpiece conformation, correlating with Mn^{2+}-induced conversion of rolling adhesion to firm adhesion (16). Binding of ligand to some integrins, such as RGD binding to $\alpha_V\beta_3$ and $\alpha_{IIb}\beta_3$, induces the open headpiece conformation (41). The lack of such induction of the open headpiece by MAdCAM binding may be functionally important to support rolling adhesion over vascular surfaces and to permit subsequent signals such as chemoattractants to activate the open headpiece and firm adhesion. In headpiece opening, the ligand-binding site in the immediate vicinity of the MIDAS undergoes rearrangements of about 2 Å, and it is possible that the integrin-binding CD loop in MAdCAM could be compliant and alter in conformation between these two states. Thus, the unique flexibility of the CD loop in D1 of MAdCAM, compared with all other integrin IgSF ligands (19), may specialize it to mediate both rolling and firm adhesion. However, we do not propose that any of the loop conformations identified here correspond to these two states, and we believe that further change from a state resembling the PF-547659-bound state occurs during integrin binding as described above. A caveat to this hypothesis is that VCAM can also mediate both rolling and firm adhesion (42), and it is possible that flexibility of the CD loop in MAdCAM-1 may be more important to enhance the rate of

[3] H. Sun and J. Chen, personal communication.

receptor-ligand encounter in shear flow, as described above. Further structural and kinetic studies are required to test these ideas.

The interaction of $\alpha_4\beta_7$ with MAdCAM is an important therapeutic target. Antibody natalizumab to α_4 is approved for Crohn disease (43), and vedolizumab specific for $\alpha_4\beta_7$ is advancing in human trials (44). Targeting MAdCAM is an alternative and highly specific method of treating inflammatory bowel disease. PF-547659 is a fully human antibody that shows potential utility in first-in-human ulcerative colitis trials (25, 45). Both 10G3 and PF-547659 are potent blockers of $\alpha_4\beta_7$ binding to MAdCAM *in vitro* (25, 35). Our crystal structures show that these Fabs bind to distinct epitopes in D1, with PF-547659 binding to the N-terminal tip of D1, and 10G3 engaging the β-sheet edge of D1 bearing the CD loop. Based on docking of VCAM and MAdCAM to $\alpha_4\beta_7$ (16), each antibody is expected to directly occlude binding of D1 to $\alpha_4\beta_7$. The Fab complexes thus illuminate mechanisms for preventing inflammatory bowel disease *in vivo*, as well as novel insights into the fold and unique dynamic flexibility of the integrin-binding loop of D1 of MAdCAM.

Acknowledgments—We thank Drs. Gang Song and Yuting Yang for purification, crystallization, and initial refinement of wild-type MAdCAM at 1.7 Å. We also thank the staff at Advanced Photon Source GM/CA beamline.

REFERENCES

1. Briskin, M. J., McEvoy, L. M., and Butcher, E. C. (1993) MAdCAM-1 has homology to immunoglobulin and mucin-like adhesion receptors and to IgA1. *Nature* **363,** 461–464
2. Streeter, P. R., Berg, E. L., Rouse, B. T., Bargatze, R. F., and Butcher, E. C. (1988) A tissue-specific endothelial cell molecule involved in lymphocyte homing. *Nature* **331,** 41–46
3. Berlin, C., Berg, E. L., Briskin, M. J., Andrew, D. P., Kilshaw, P. J., Holzmann, B., Weissman, I. L., Hamann, A., and Butcher, E. C. (1993) $\alpha_4\beta_7$ integrin mediates lymphocyte binding to the mucosal vascular addressin MAdCAM-1. *Cell* **74,** 185–195
4. Springer, T. A. (1994) Traffic signals for lymphocyte recirculation and leukocyte emigration. The multi-step paradigm. *Cell* **76,** 301–314
5. Shimaoka, M., Xiao, T., Liu, J.-H., Yang, Y., Dong, Y., Jun, C.-D., McCormack, A., Zhang, R., Joachimiak, A., Takagi, J., Wang, J.-H., and Springer, T. A. (2003) Structures of the αL I domain and its complex with ICAM-1 reveal a shape-shifting pathway for integrin regulation. *Cell* **112,** 99–111
6. Chen, X., Kim, T. D., Carman, C. V., Mi, L. Z., Song, G., and Springer, T. A. (2007) Structural plasticity in IgSF domain 4 of ICAM-1 mediates cell surface dimerization. *Proc. Natl. Acad. Sci. U.S.A.* **104,** 15358–15363
7. Bella, J., Kolatkar, P. R., Marlor, C. W., Greve, J. M., and Rossmann, M. G. (1998) The structure of the two amino-terminal domains of human ICAM-1 suggests how it functions as a rhinovirus receptor and as an LFA-1 integrin ligand. *Proc. Natl. Acad. Sci. U.S.A.* **95,** 4140–4145
8. Casasnovas, J. M., Springer, T. A., Liu, J.-H., Harrison, S. C., and Wang, J.-H. (1997) The crystal structure of ICAM-2 reveals a distinctive integrin recognition surface. *Nature* **387,** 312–315
9. Song, G., Yang, Y., Liu, J.-H., Casasnovas, J. M., Shimaoka, M., Springer, T. A., and Wang, J.-H. (2005) An atomic resolution view of ICAM recognition in a complex between the binding domains of ICAM-3 and integrin $\alpha_L\beta_2$. *Proc. Natl. Acad. Sci. U.S.A.* **102,** 3366–3371
10. Zhang, H., Casasnovas, J. M., Jin, M., Liu, J. H., Gahmberg, C. G., Springer, T. A., and Wang, J. H. (2008) An unusual allosteric mobility of the C-terminal helix of a high-affinity αL integrin I domain variant bound to ICAM-5. *Mol. Cell* **31,** 432–437
11. Jones, E. Y., Harlos, K., Bottomley, M. J., Robinson, R. C., Driscoll, P. C., Edwards, R. M., Clements, J. M., Dudgeon, T. J., and Stuart, D. I. (1995) Crystal structure of an integrin-binding fragment of vascular cell adhesion molecule-1 at 1.8 Å resolution. *Nature* **373,** 539–544
12. Wang, J. H., Pepinsky, R. B., Stehle, T., Liu, J. H., Karpusas, M., Browning, B., and Osborn, L. (1995) The crystal structure of an N-terminal two-domain fragment of (VCAM-1). A cyclic peptide based on the domain 1 C-D loop can inhibit VCAM-1-α4 integrin interaction. *Proc. Natl. Acad. Sci. U.S.A.* **92,** 5714–5718
13. Green, N., Rosebrook, J., Cochran, N., Tan, K., Wang, J. H., Springer, T. A., and Briskin, M. J. (1999) Mutational analysis of MAdCAM-1/$\alpha4\beta7$ interactions reveals significant binding determinants in both the first and second immunoglobulin domains. *Cell Adhes. Commun.* **7,** 167–181
14. Briskin, M. J., Rott, L., and Butcher, E. C. (1996) Structural requirements for mucosal vascular addressin binding to its lymphocyte receptor $\alpha_4\beta_7$. Common themes among integrin-Ig family interactions. *J. Immunol.* **156,** 719–726
15. Newham, P., Craig, S. E., Seddon, G. N., Schofield, N. R., Rees, A., Edwards, R. M., Jones, E. Y., and Humphries, M. J. (1997) α_4 integrin binding interfaces on VCAM-1 and MAdCAM-1. Integrin binding footprints identify accessory binding sites that play a role in integrin specificity. *J. Biol. Chem.* **272,** 19429–19440
16. Yu, Y., Zhu, J., Mi, L. Z., Walz, T., Sun, H., Chen, J., and Springer, T. A. (2012) Structural specializations of $\alpha_4\beta_7$, an integrin that mediates rolling adhesion. *J. Cell Biol.* **196,** 131–146
17. Berg, E. L., McEvoy, L. M., Berlin, C., Bargatze, R. F., and Butcher, E. C. (1993) L-selectin-mediated lymphocyte rolling on MAdCAM-1. *Nature* **366,** 695–698
18. Tan, K., Casasnovas, J. M., Liu, J.-H., Briskin, M. J., Springer, T. A., and Wang, J.-H. (1998) The structure of immunoglobulin superfamily domains 1 and 2 of MAdCAM-1 reveals novel features important for integrin recognition. *Structure* **6,** 793–801
19. Wang, J., and T. A. Springer, T. A. (1998) Structural specializations of immunoglobulin superfamily members for adhesion to integrins and viruses. *Immunol. Rev.* **163,** 197–215
20. Dando, J., Wilkinson, K. W., Ortlepp, S., King, D. J., and Brady, R. L. (2002) A reassessment of the MAdCAM-1 structure and its role in integrin recognition. *Acta Crystallogr. D Biol. Crystallogr.* **58,** 233–241
21. Taylor, P., Bilsland, M., and Walkinshaw, M. D. (2001) A new conformation of the integrin-binding fragment of human VCAM-1 crystallizes in a highly hydrated packing arrangement. *Acta Crystallogr. D Biol. Crystallogr.* **57,** 1579–1583
22. Huang, P. S., Ban, Y. E., Richter, F., Andre, I., Vernon, R., Schief, W. R., and Baker, D. (2011) RosettaRemodel. A generalized framework for flexible backbone protein design. *PLoS One* **6,** e24109
23. Dukkipati, A., Park, H. H., Waghray, D., Fischer, S., and Garcia, K. C. (2008) BacMam system for high-level expression of recombinant soluble and membrane glycoproteins for structural studies. *Protein Expr. Purif.* **62,** 160–170
24. Reeves, P. J., Thurmond, R. L., and Khorana, H. G. (1996) Structure and function in rhodopsin. High level expression of a synthetic bovine opsin gene and its mutants in stable mammalian cell lines. *Proc. Natl. Acad. Sci. U.S.A.* **93,** 11487–11492
25. Pullen, N., Molloy, E., Carter, D., Syntin, P., Clemo, F., Finco-Kent, D., Reagan, W., Zhao, S., Kawabata, T., and Sreckovic, S. (2009) Pharmacological characterization of PF-00547659, an anti-human MAdCAM monoclonal antibody. *Br. J. Pharmacol.* **157,** 281–293
26. Kabsch, W. (2001) *International Tables for Crystallography* (Rossmann, M. G., and Arnold, E., eds) Vol. F, pp. 730–734, Kluwer Academic Publishers, Dordrecht, The Netherlands
27. Minor, W., Cymborowski, M., Otwinowski, Z., and Chruszcz, M. (2006) HKL-3000: the integration of data reduction and structure solution–from diffraction images to an initial model in minutes. *Acta Crystallogr. D Biol. Crystallogr.* **62,** 859–866
28. McCoy, A. J., Grosse-Kunstleve, R. W., Adams, P. D., Winn, M. D., Storoni, L. C., and Read, R. J. (2007) Phaser crystallographic software. *J. Appl. Crystallogr.* **40,** 658–674
29. Emsley, P., and Cowtan, K. (2004) Coot. Model-building tools for molec-

ular graphics. *Acta Crystallogr. D Biol. Crystallogr.* **60,** 2126–2132
30. Murshudov, G. N., Vagin, A. A., and Dodson, E. J. (1997) Refinement of macromolecular structures by the maximum-likelihood method. *Acta Crystallogr. D Biol. Crystallogr.* **53,** 240–255
31. Adams, P. D., Grosse-Kunstleve, R. W., Hung, L. W., Ioerger, T. R., McCoy, A. J., Moriarty, N. W., Read, R. J., Sacchettini, J. C., Sauter, N. K., and Terwilliger, T. C. (2002) PHENIX: building new software for automated crystallographic structure determination. *Acta Crystallogr. D Biol. Crystallogr.* **58,** 1948–1954
32. Davis, I. W., Leaver-Fay, A., Chen, V. B., Block, J. N., Kapral, G. J., Wang, X., Murray, L. W., Arendall, W. B., 3rd, Snoeyink, J., Richardson, J. S., and Richardson, D. C. (2007) MolProbity. All-atom contacts and structure validation for proteins and nucleic acids. *Nucleic Acids Res.* **35,** W375–W383
33. van den Bedem, H., Lotan, I., Latombe, J. C., and Deacon, A. M. (2005) Real-space protein-model completion. An inverse-kinematics approach. *Acta Crystallogr. D Biol. Crystallogr.* **61,** 2–13
34. Janin, J. (1997) Specific *versus* nonspecific contacts in protein crystals. *Nat. Struct. Biol.* **4,** 973–974
35. Briskin, M., Winsor-Hines, D., Shyjan, A., Cochran, N., Bloom, S., Wilson, J., McEvoy, L. M., Butcher, E. C., Kassam, N., Mackay, C. R., Newman, W., and Ringler, D. J. (1997) Human mucosal addressin cell adhesion molecule-1 is preferentially expressed in intestinal tract and associated lymphoid tissue. *Am. J. Pathol.* **151,** 97–110
36. Lo Conte, L., Chothia, C., and Janin, J. (1999) The atomic structure of protein-protein recognition sites. *J. Mol. Biol.* **285,** 2177–2198
37. Viney, J. L., Jones, S., Chiu, H. H., Lagrimas, B., Renz, M. E., Presta, L. G., Jackson, D., Hillan, K. J., Lew, S., and Fong, S. (1996) Mucosal addressin cell adhesion molecule-1. A structural and functional analysis demarcates the integrin-binding motif. *J. Immunol.* **157,** 2488–2497
38. Chiu, H. H., Crowe, D. T., Renz, M. E., Presta, L. G., Jones, S., Weissman, I. L., and Fong, S. (1995) Similar but nonidentical amino acid residues on vascular cell adhesion molecule-1 are involved in the interaction with $\alpha_4\beta_1$ and $\alpha_4\beta_7$ under different activity states. *J. Immunol.* **155,** 5257–5267
39. Baerga-Ortiz, A., Rezaie, A. R., and Komives, E. A. (2000) Electrostatic dependence of the thrombin-thrombomodulin interaction. *J. Mol. Biol.* **296,** 651–658
40. Chen, J., Salas, A., and Springer, T. A. (2003) Bistable regulation of integrin adhesiveness by a bipolar metal ion cluster. *Nat. Struct. Biol.* **10,** 995–1001
41. Springer, T. A., and Dustin, M. L. (2012) Integrin inside-out signaling and the immunological synapse. *Curr. Opin. Cell Biol.* **24,** 107–115
42. Alon, R., Kassner, P. D., Carr, M. W., Finger, E. B., Hemler, M. E., and Springer, T. A. (1995) The integrin VLA-4 supports tethering and rolling in flow on VCAM-1. *J. Cell Biol.* **128,** 1243–1253
43. Sandborn, W. J., Colombel, J. F., Enns, R., Feagan, B. G., Hanauer, S. B., Lawrance, I. C., Panaccione, R., Sanders, M., Schreiber, S., Targan, S., van Deventer, S., Goldblum, R., Despain, D., Hogge, G. S., Rutgeerts, P., International Efficacy of Natalizumab as Active Crohn's Therapy (ENACT-1) Trial Group, and Evaluation of Natalizumab as Continuous Therapy (ENACT-2) Trial Group (2005) Natalizumab induction and maintenance therapy for Crohn's disease. *N. Engl. J. Med.* **353,** 1912–1925
44. Parikh, A., Leach, T., Wyant, T., Scholz, C., Sankoh, S., Mould, D. R., Ponich, T., Fox, I., and Feagan, B. G. (2012) Vedolizumab for the treatment of active ulcerative colitis. A randomized controlled phase 2 dose-ranging study. *Inflamm. Bowel Dis.* **18,** 1470–1479
45. Vermeire, S., Ghosh, S., Panes, J., Dahlerup, J. F., Luegering, A., Sirotiakova, J., Strauch, U., Burgess, G., Spanton, J., Martin, S. W., and Niezychowski, W. (2011) The mucosal addressin cell adhesion molecule antibody PF-00547,659 in ulcerative colitis. A randomised study. *Gut* **60,** 1068–1075
46. Sun, H., Wu, Y., Qi, J., Pan, Y., Ge, G., and Chen, J. (2011) The CC′ and DE loops in Ig domains 1 and 2 of MAdCAM-1 play different roles in MAdCAM-1 binding to low- and high-affinity integrin $\alpha4\beta7$. *J. Biol. Chem.* **286,** 12086–12092